The Dynamics of the Human Head During Natural Activities that Require Clear Vision
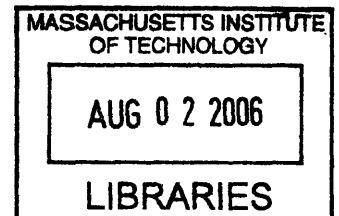
by

Warren Bates

SUBMITTED TO THE DEPARTMENT OF MECHANICAL ENGINEERING IN PARTIAL FULFILLMENT OF THE REQUIREMENTS FOR THE DEGREE OF

BACHELOR OF SCIENCE
AT THE
MASSACHUSETTS INSTITUTE OF TECHNOLOGY

JUNE 2006

Signature of Author:_____
Department of Mechanical Engineering
May 12, 2006

Certified by:_____
Dr. Lynette Jones
Principal Research Scientist, MIT Bioinstrumentation Lab
Thesis Co-Supervisor

Certified by:_____
Dr. James Tangorra
Post/Doctoral Associate, MIT Bioinstrumentation Lab
Thesis Co-Supervisor

Accepted by:_____
John H. Lienhard V
Professor of Mechanical Engineering
Chairman, Undergraduate Thesis Committee

ARCHIVES

The Dynamics of the Human Head During
Natural Activities that Require Clear Vision

by

Warren W. Bates

Submitted to the Department of Mechanical Engineering
on May 12, 2006 in Partial Fulfillment of the
Requirements for the Degree of Bachelor of Science in
Mechanical Engineering

ABSTRACT

The current understanding of the dynamics of the human head, and the demands placed on its control and stability systems, is based largely on the results of experiments conducted in artificial settings, such as when subjects are tasked with walking or running in place, and may not reflect the dynamics of the head during normal behaviors. The objective of this research was to quantify the dynamics of the head during natural activities that require clear vision and to establish input-output relations between the trunk's motion and the head's response. A portable sensor and data acquisition system was developed using MEMs based angular velocity sensors to track the yaw and pitch velocities of the head and the trunk. Subjects were tested under experimental conditions that required them to 1) simultaneously walk or run, and visually track and catch a moving ball, 2) walk or run without being given a defined visual task, and 3) stand in place and maintain eye contact with the experimenter during a conversation. During all trials, head velocities rarely exceeded 160 deg/s in pitch and 200 deg/s in yaw, and trunk velocities rarely exceeded 90 deg/s in pitch and 200 deg/s in yaw. In yaw, head and trunk velocities were greatest when subjects ran without a defined visual task. The velocities of the head and trunk decreased considerably when subjects had to also track and catch the moving ball. This reduction was in spite of subjects running approximately 50% faster than when no visual task had been given, and likely reflects the need to stabilize the head against yaw motions to maintain clear vision. Surprisingly, the results were reversed for pitch velocities. Larger magnitude head and trunk velocities occurred in pitch when subjects ran and visually tracked the ball's trajectory than when subjects ran without the visual task. For all conditions, the frequency spectra of head and trunk velocities were dominated by power between 0.0 and 2.0 Hz, with the power spectral density dropping by more than three orders of magnitude by 10.0 Hz.

Thesis Supervisor: Dr. James Tangorra
Title: Post-Doctoral Associate

TABLE OF CONTENTS

1 Introduction

The goal of this research was to develop the proper equipment, testing protocol, and analysis algorithms to evaluate the angular velocity of the human head and trunk during unrestrained, natural activities that require clear vision.

The human head serves as the platform for the sensory systems that allow us to interact with the world, including the visual, auditory, and vestibular systems. The maneuverability and stability of the head and neck affect how well these systems, and therefore humans, interact with the environment. The head must move well so that its sensory systems can be positioned to best interact with the environment and be well stabilized so that it can resist disturbances to its position caused by undesired movements of the trunk. Head stability is particularly important because of its potential effect on vision. A disturbance in head motion can cause the eyes to move away from a visual target. The vestibular ocular reflex (VOR) stabilizes vision by moving the eyes equal and opposite to disturbances in head motion. However, the VOR is effective only over a limited bandwidth and range of head velocity. The head must therefore be stabilized well enough so that its velocities and frequencies do not exceed the ability of the VOR to make corrective eye motions.

Motivations for studying the head-neck system include furthering our understanding of the human vestibular system, providing information about head motions for human factors research, and contributing to military research. Vestibular dysfunction is very common in Americans, especially those over 65 years old. In fact, "Over 90 million Americans, age 17 and older, have experienced a dizziness or balance problem," while over 30% of persons age 65-75, reported imbalance and dizziness "degraded their

Some of the most modern testing protocols evaluate vestibular performance by using active and passive movements of the head for a stimulus to the vestibular system. It is therefore necessary to understand the movement experienced by the head if testing protocols are to recreate accurately the conditions experienced by the vestibular system in real life.

Head dynamics have been a particular interest of the U.S. military and its allies because they can change when heavy equipment is attached to a soldier's head (i.e. communication devices, night vision goggles, extra-strength bulletproof materials). According to Professor Michael Worswick of the University of Waterloo, "Theoretically, one can design a helmet that will stop virtually anything but it would be so huge and heavy a soldier would not be able to walk around with it on. In addition to providing protection, the helmet must also permit mobility -- it must be reasonably small in size and low in weight, which can affect the ability of the soldier to compensate for unwanted head movements" (Whitton, 1999). To design helmets properly, the U.S. military must understand how the head is used and how its ability to move and be stabilized are affected by weight.

Unfortunately, our current understanding of the dynamics of the head is primarily based upon experiments done in artificial laboratory settings. For example, Grossman *et. al* (1988) determined the frequency and velocity of rotational head perturbations in four conditions: walking in place, running in place, "during vigorous, voluntary, horizontal head rotations", and "during vigorous, voluntary vertical head rotations". They found that the maximum velocities in the horizontal and vertical directions were in the order of 1100 and 700 deg/s, respectively. This study accurately described the dynamics of the

place" or voluntarily shaking your head do not necessarily recreate closely the natural

movements of a human. Other studies that use contrived exercises include Pozzo *et. al*

(1990, walking, walking in place, running in place, and hopping), Pulaski *et. al* (1981;

voluntary, horizontal head movements while seated in a moving chair), Fuller (1992;

voluntary, horizontal head movements), and Pozzo *et. al* (1995; standing on a narrow

beam and an unstable, rocking platform).

The goal of this research was to develop the proper equipment and testing

protocol to evaluate the angular velocity of human head and trunk movements during

unrestrained, natural activities requiring clear vision. Human subjects were instrumented

with angular rate sensors on their head and trunk which were used to measure velocity in

the pitch (rotation in sagittal plane) and yaw direction (rotation in transverse plane).

Equipment was developed that allowed for unrestrained movement of the head and trunk

during the experiments so the results reflected a full range of movement. Subjects were

tested under experimental conditions that required them to 1) simultaneously walk or run,

and visually track and catch a moving ball, 2) walk or run without being given a defined

visual task, and 3) stand in place and maintain eye contact with the experimenter during a

conversation. Tossing a "fly ball" in the air to a spot away from the start point of the

subject was one of the best ways to accomplish the testing protocol objectives. These

experiments are an important step towards determining the dynamics of the head and

trunk and developing a model that represents the response of the head to movements of

the trunk during natural activities.

2 Equipment

The major design objectives for the experimental equipment were to develop an integrated system that would allow for the yaw and pitch of the head and trunk to be measured and to prevent the equipment from interfering with the subject's full range of motion. The experimental equipment consisted of three main elements (Figure 1): 1) a lightweight helmet with two angular rate sensors, one for yaw and one for pitch, 2) a waist mounted sensor pack to measure the angular rate of trunk, and 3) a portable data acquisition system carried in a backpack. This setup allowed the head and trunk to be measured so that the head's response could be compared to the movements of the body. In addition, the portability of the system allowed for freedom of motion for the trunk and the head.
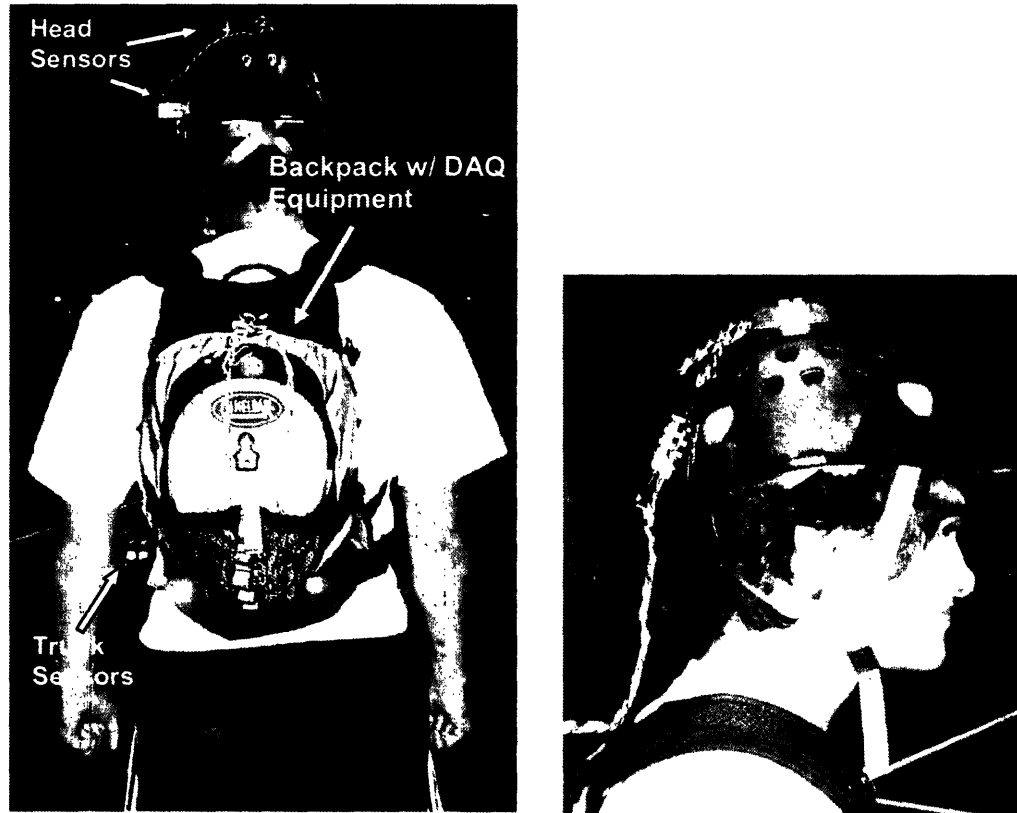
Figure 1: Experimental equipment (DAQ system located in backpack)

The angular rate sensors were Analog Devices iMEMS® gyroscopes (Model ADXRS300, Figure 2) that were built to operate over a range of -300 to +300 deg/s. This range could be altered simply by changing the resistance of the angular rate sensor circuit (Analog Devices Application Note AN-625). Based on previous studies (Grossman et al, 1988; Pozzo et al, 1990), +/- 300 deg/s was selected as an appropriate operating range. Each chip contained all necessary amplification and filtering so there was no need to further amplify and/or filter the signal output from each sensor. Specifically, there is a single-pole 40 Hz low-pass filter that limits high frequency signals before the final amplification takes place. The sensor varies its output from 0.0 V to 5.0 V as the sensor rotates between -300 deg/s and +300 deg/s, respectively.

Power was supplied via a 5 V regulator from Radioshack (Model 7805) and 4 AA Duracell batteries, which provided 6 V of power and were carried in a simple battery pack (Figure 3). The current consumption of each sensor was 6.0 to 8.0 mA. Additional specifications for the sensors and associated components are listed in Appendices A, B, and C. The sensors were connected to the voltage regulators and soldered to circuit boards so the output signals could be measured (Figure 2).

Figure 2: PC boards with ADXRS300 evaluation board and voltage regulator
(Measurements: 49.4mm x 27.4m; 9.36 grams)

Figure 3: Battery pack

Based on energy density calculations, it was determined that 4 AA batteries would be sufficient to run four angular rate sensors continuously for 164 hours. This was clearly ample time to conduct long duration tests with subjects. An energy density of 515 x 10^3 J/kg for each battery was determined from the manufacturer (Duracell, Appendix D). A usage time of 164 hours was estimated by the following calculations.

$$DuracellAAEnergyDensity = 143Wh/kg = 515 \times 10^3 J/kg$$

Each AA battery provides 1.5 volts,

therefore 4 AA batteries in series provide 4 x 1.5 volts = 6 volts.

Each sensor requires a max of 0.007 amp.

Power for each sensor,

$$P = VI = 6volts(.007Amps) = 0.042W = 0.042J/s.$$

Each battery has a mass of 0.024 kg and holds 515 x 10^3 J/kg. Therefore,

$$E/battery = 515 \times 10^3 J/kg(0.024kg) = 12,360Joules$$

and $E_{predicted} = 4 \times 12,360Joules = 49,440Joules$.

Assuming 50% efficiency,

$$E_{actual} = E_{predicted} \times 0.5 = 24,720Joules.$$

Finally,

$$Total\_Running\_Time = E_{actual} / P = 24,720J /(0.042J/s) \approx 590 \times 10^3 s$$

$$\therefore Total\_Running\_Time \approx 590,000s = 9,833 \min = 164 hrs.$$

2.1 Helmet Designs

The angular rate sensors for the head were attached to an adjustable Petzl climbing helmet (Petzl Model ECRIN-ROC, Figure 4). A climbing helmet was selected over other mounting methods, such as a head band, because it could be easily adjusted to fit many subjects, could be made snug so that it did not slip when the subject's head moved, and its shell provided a rigid surface onto which the sensors could be mounted.

Figure 4: *Complete helmet apparatus with side-mounted head pitch and top-mounted head yaw sensors connected to junction box in back*

A challenge in constructing the head sensor system was mounting the pitch and yaw sensors to the helmet so that they were adjustable to fit each subject correctly, made tight, and done so in a manner that did not hold too much weight. Also, the sensor

(Figure 2) needed to be protected from inclement weather, as well as, unexpected impacts such as a subject falling or the helmet being dropped. To do so, each was mounted in an acrylic box. The boxes were designed depending on the application (head or trunk) using CAD software (Solid Edge) and then constructed with 3mm acrylic, which was cut using a Trotec laser cutter in MIT's Bioinstrumentation Lab. The sensors were mounted to the acrylic box with screws and spacers (nylon washers) so that the boards sat off of the acrylic. Epoxy and 1.6mm screws were used to seal the acrylic boxes (Figure 5).

The first design mounted two sensor boards (yaw and pitch) at right angles in a single acrylic box that attached to the top of the helmet. Construction was completed, and the box measured 70.1 x 50.3 x 50.3mm (Figure 5). A key requirement in the mounting process was that the helmet sensors were easily adjustable. Since all subjects wore the helmet differently, the sensors had to be able to be adjusted so that the sensors could be made parallel to the horizontal (yaw) and vertical (pitch) planes. On this design (Figure 6) a cradle was used that attached to the top of the helmet. This cradle allowed the sensor box to be rotated in pitch and tightened when parallel to the ground. However, the sensors and the box, which weighed 0.0866 kg, were located about 90 mm above the top of each subject's head and made the helmet feel "top heavy" and uncomfortable. The weight seemed to matter only when the subject was tilting their head back. No testing was done to quantify if this altered the dynamics of the head, but it was clear from surveying multiple subjects that a helmet that was lighter or had a lower center of gravity would be preferred.

11
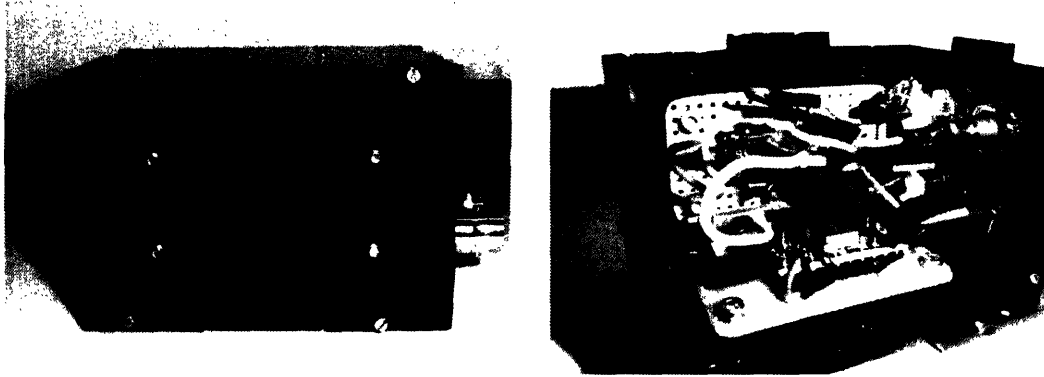
Figure 5: Outside and inside of first sensor box design
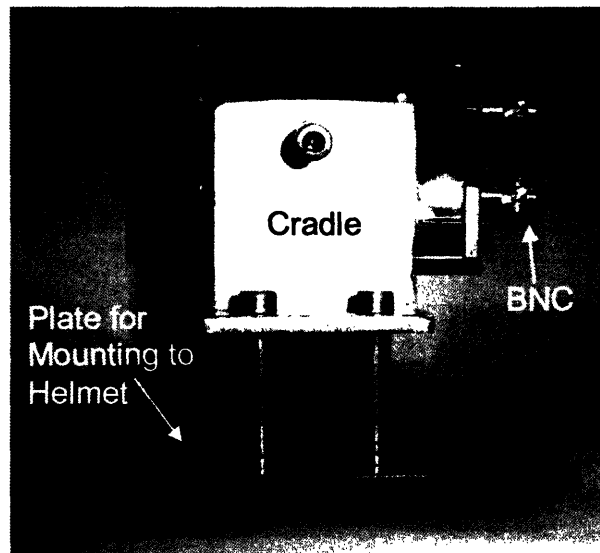
Figure 6: Head mounting design I

A second design (II) had to meet two major design objectives – easily adjustable boxes and a lower center of gravity. Two sensors in the same box aligned at a right angle force it to be the size of the first box, so it was decided to separate the sensors and mount one on the top (yaw) and one on the side (pitch) of the helmet. Overall, this would give the helmet a lower center of gravity with the goal being a negligible and unnoticeable change to head dynamics while in use.

The two sensor II boxes were identical, and one can be seen in Figure 7. To further decrease the size of these boxes, the BNC and power connections were all combined into a junction box on the rear of the helmet (Figure 8). Therefore, only wires would exit each new sensor box, allowing the sensor boxes to be built at smaller heights. This junction box served as the point where the wires from the head yaw and head pitch sensor boxes could meet, and the connections made to the data acquisition equipment.

Figure 7: Head yaw sensor mounted on top of helmet

Figure 8: Junction box mounted on back of helmet

This new design has noticeably lowered the center of gravity of the helmet because the yaw and pitch sensors are now mounted much closer to the head while maintaining similar mass from that of design I. The actual center of gravity was not

calculated, but it was roughly determined by balancing the helmet. Moreover, the same people who wore design I, reported that there was there was an obvious improvement in the helmet-sensor system. Many even said they could not notice the helmet after wearing it for several minutes. After many positive reactions from everyone surveyed, we were convinced that this design would suffice. While there are always improvements that could be made to lighten the helmet or lower its profile, we believe this design is a good base for future data collection.

2.2 Trunk Mounting

The angular rate sensors for the trunk were attached to a nylon-webbed belt (Figure 9). A waist belt was selected over other mounting methods, such as a chest strap, because it provided the least obstruction to movement and could be made snug so it did not slip during motion.

The major issues in the design of the trunk attachment were the location of the sensor box and the elasticity of the strap used for the belt. Because the size of the box was less critical than for the head, it was decided that the sensor box from helmet design I could conveniently be used for this application. At first, the chest was the location chosen for the box, and an elastic strap was used to keep it attached at the same point. Testing proved this to be a bad combination. In order for the sensors to be aligned to properly measure the yaw and pitch axes, the box would be attached with its smallest side (50.3 x 50.3mm) against the chest. Furthermore, this orientation would force the BNC and power wires to come out from the subject's chest when connected. Not only was this unstable because the box stuck out 70.1mm from the chest, but the wires inhibit the subject's motion, thereby defeating the purpose of the experiment. The easy solution of

re-using the first helmet design box no longer seemed to make sense. Moreover, the elastic strap allowed too much stretching while walking or running. This elasticity caused the box to continue to accelerate when the body came to a stop.

Instead of rebuilding, these problems were corrected by placing the sensor box at the side of the test subject using a nylon-webbed belt, thereby solving both problems. By attaching to the left side of a subject's abdomen, the long side of the box could be held tightly to the body with the wires attaching in the back. This allowed for unrestrained motion and a better fit than before. In addition, the nylon-webbed belt provided a rigid fit so the elasticity issue was improved. Figure 10 shows the final attachment that was utilized for the testing. The ability to move unrestricted is evident in the photo.
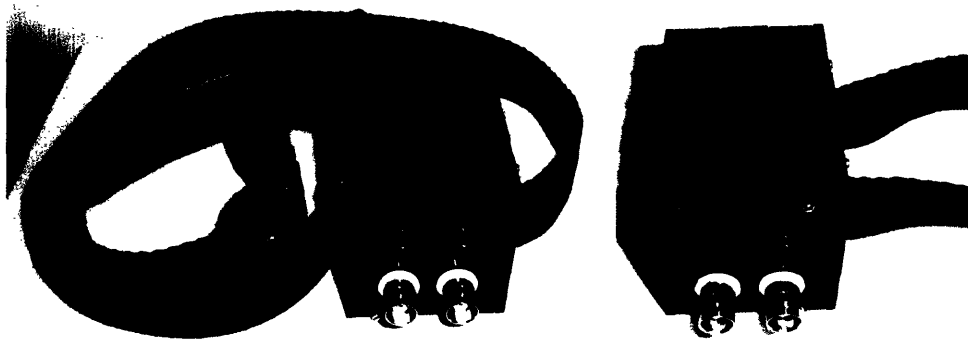
Figure 9: Trunk belt with 2-D sensor box attached

Figure 10: Trunk attachment on subject during testing

The final dimensions of the acrylic boxes can be viewed in Table 1.

Box	Head Pitch	Head Yaw	Trunk 2-D	Junction
Size (mm)	70.7 x 50.3 x 24.1	70.7 x 50.3 x 24.1	70.1 x 50.3 x 50.3	54.7 x 29.8 x 24.1
Mass (kg)	0.0456	0.0456	0.0866	0.0566

Table 1: Acrylic box dimensions (in millimeters) and mass (in kg)

2.3 DAQ

A data acquisition (DAQ) system was necessary to convert the output signals from the sensors to readable information on a PC. Our toughest challenge was creating a DAQ system that would allow the test subject to move freely and over great distances. In order to do this, it was imperative that no wires tethered the subject to a stationary DAQ system. One option emerged as the best way to reach our goal – a portable data acquisition site that was carried by the subject. Designed properly, there would be no restrictions on movement and no chance of injury through tripping over long wires while running. However, there were some potential problems with this setup. Comfort and not affecting the motion of the trunk had become issues since the plan was now to strap a potentially heavy DAQ connection block and PC to each subject. Choosing a proper PC became important because any extra weight could change a subjects' dynamics. Moreover, a typical laptop shuts off when the lid is closed, so a solution for that was necessary to collect data during testing. These design specs were all critical in reaching the goal of the experiment.

The DAQ system included both hardware and software from National Instruments. The hardware used to acquire data included a National Instruments SCB-68 Shielded I/O Connector Block with 68-pin connectors and a NI DAQCard-6063E. The

BNC connectors from the sensor boxes were converted back to wires and connected into

the SCB-68. Out of the other end of the SCB-68 exits a wire that connects to the

DAQCard, which is displayed in Figure 11. With the help of a strain relief tool that is

glued to the tablet PC, the DAQCard is placed in the PCMCIA slot and the data is

transmitted to the computer through data acquisition software (LabVIEW).
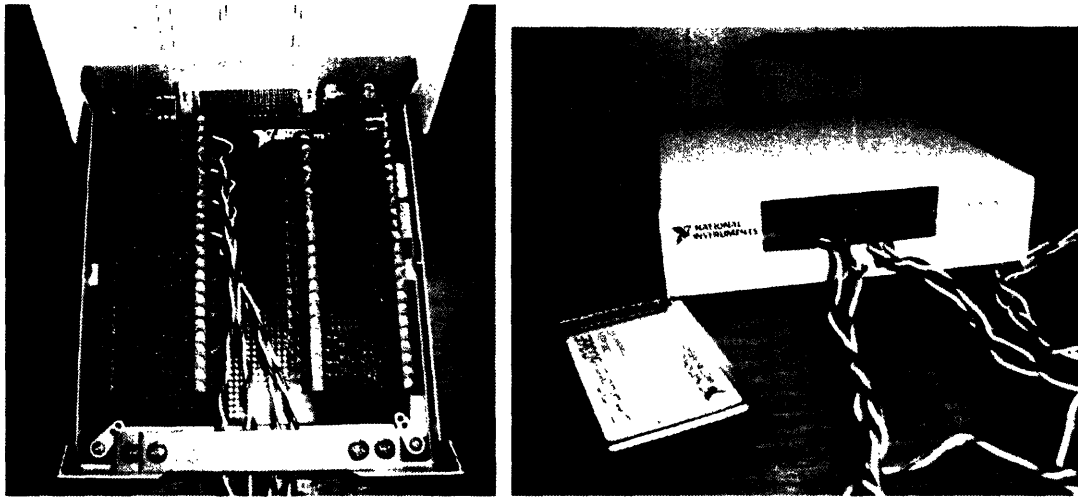
Figure 11: Inside and outside views of the NI SCB-68 and DAQCard

At this point, the type of computer was an important issue in the DAQ setup. The

objective was to find a type of computer that weighs as little as possible and can take data

with the lid closed. A solution was apparent almost immediately – a tablet PC. On

average, they are smaller and lighter than a regular laptop, and there is no lid to close so

data can be collected in the closed backpack on the tablet PC. The tablet PC used in this

experiment was made by Motion Computing.

A backpack was purchased and altered to house the tablet PC, data acquisition

equipment, and power supply. Specifically, a Camelbak cycling/hiking backpack was

chosen because of its lightweight, small, and easily adjustable design. One of the specifications we had to meet was to allow the PC to be easily removed from the backpack between trials to check data and adjust settings. However, we also needed to make sure the DAQ system and PC sat in the backpack tightly so they did not shake around during activity, thus imposing larger forces on the body and altering its dynamics. Moreover, we simply did not want these items to break as they are financially expensive and time intensive to fix.

Strong foam inserts were used to safely secure the objects inside the backpack. Pieces of sturdy shipping foam were cut to fit the dimensions of each of the two main pockets in the front and the back of the backpack. The tablet PC could not fit in the front pocket so it was placed in the back. The DAQ connection block was placed in a nylon pocket which was located inside the front pocket (Figure 12). The original pieces of foam were altered to accommodate the objects placed inside the pockets. Foam was added along the sides of the pockets, and an elastic tie was used to hold the PCMCIA cable in place so it did not shake or disconnect during motion. With the aid of several shoulder, chest, and waist straps attached to the backpack, the foam stabilized the data acquisition system. The backpack was then connected to the helmet and nylon belt using strategically placed BNC and power wires that allowed the subject to move freely while data was collected in the tablet PC (Figure 13).
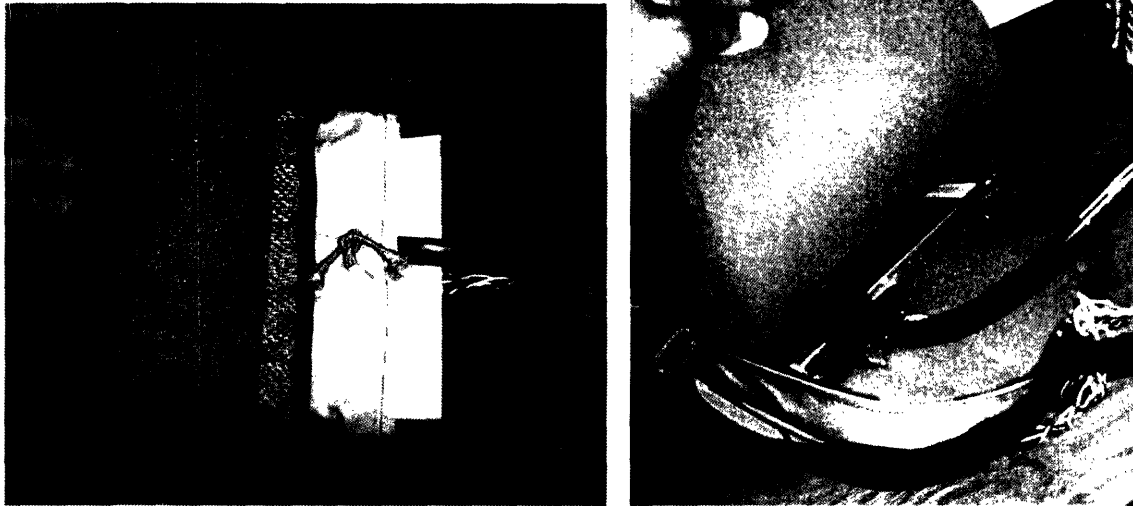
Figure 12: Front and back pockets of the backpack

*Figure 13: Outside view of backpack displaying the 4 BNC connectors and
4 power source connectors that go to the sensor boxes*

The software used to gather the data was written using LabVIEW 7.0. This DAQ program allows the user to set the DAQ rate, duration, and time delay for each data collection session. It then produces a graph showing all four channels of output. The LabVIEW block diagram and GUI are displayed in Figure 14.
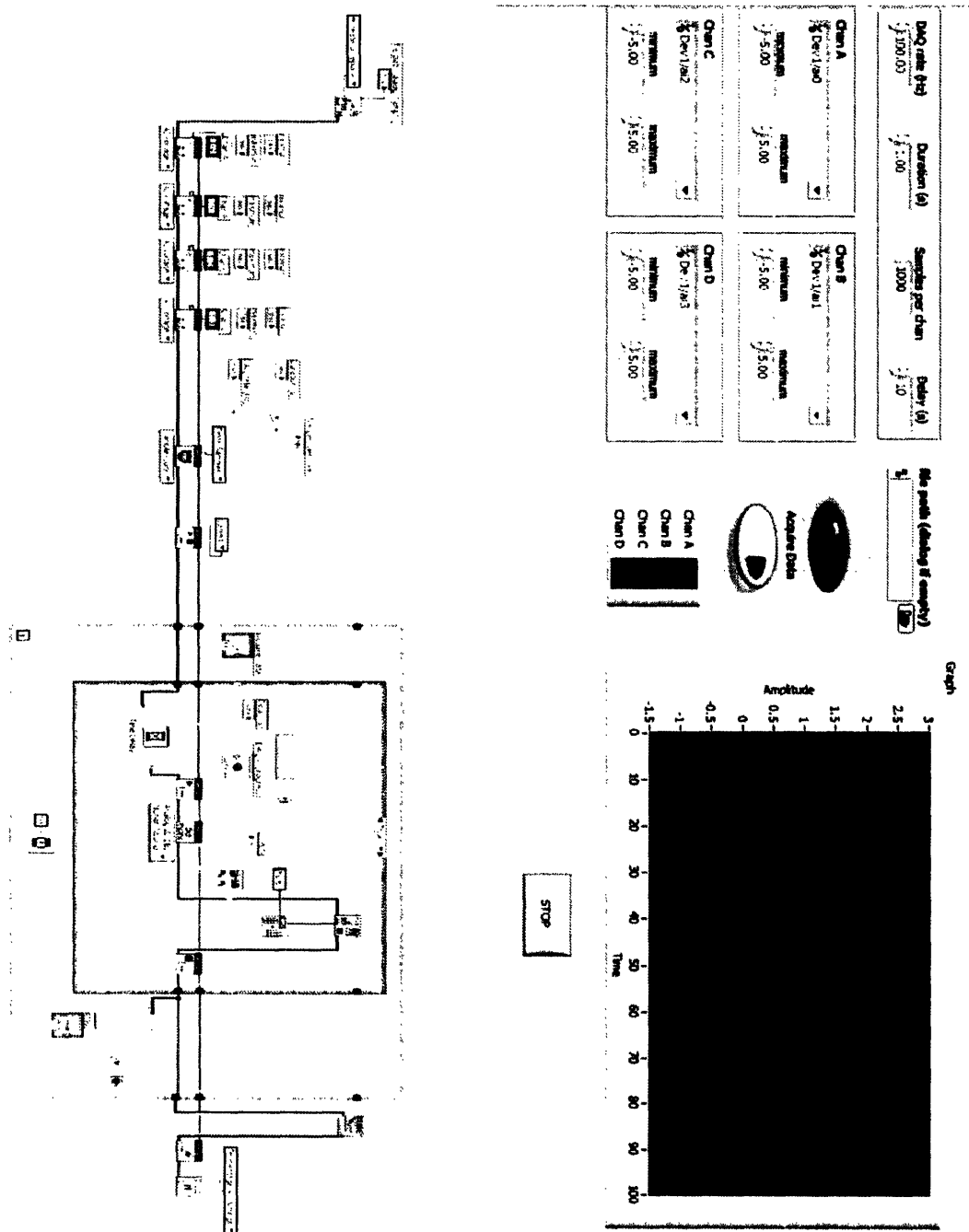

Figure 14: LabVIEW 7.0 DAQ block diagram and GUI

3 Methods

Three normal healthy subjects (1 female, 2 male), ranging in age from 19 - 22 years, with no previous history of neuromuscular disease or back injuries were examined. Their heights and weights ranged from 165 to 183 cm and 54.4 to 95.2 kg, respectively.

Subjects were instrumented with the angular accelerometers on their head and trunk using the helmet and nylon-webbed belt strap. The sensors were then connected to the data acquisition system located in the backpack worn by each subject. The backpack has several straps that were all tightened to provide the best fit possible. The front and back pockets were zipped and tied shut so there was no risk of them opening during testing.

Experimental trials were conducted by throwing a ball in four general directions: front, back, left, and right. Each trial included 12 throws – 3 forward, 3 back, 3 left and 3 right. The order of these throws was randomized so the subject did not know the direction until immediately before the throw when it was called out. Each throw was aimed to land in a 30 degree section of the centerline of each direction as shown in Figure 15. Moreover, data was acquired from subjects in between trials while they were just standing and relaxing.
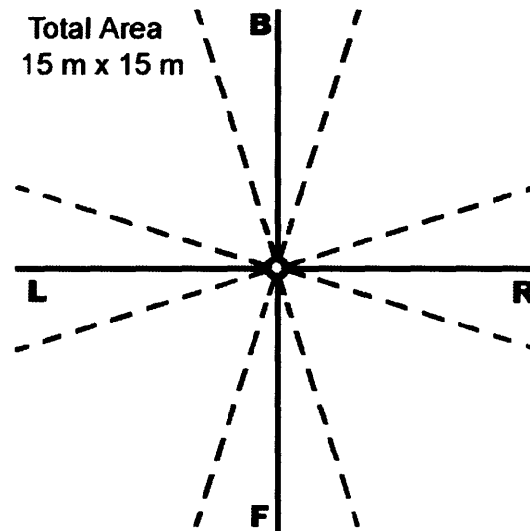
Figure 15: Experimental site layout where dotted lines represent 30 degree angles from the center line in each direction

After being instrumented properly, subjects were instructed to stand in the center of a 15 m x 15 m field. They were then told a direction immediately before being thrown the ball in that direction. A complete throw, catch, and return cycle in the trials was run in a total of 20 seconds. At t=0, a throw was executed. The subject ran and caught the ball by t=5 seconds. The subject then was stationary until instructed to throw the ball back and return to the starting position at t=10. This process took about 8 seconds. Finally, the subject remained stationary until t=20 seconds at which point the next throw was executed.

After testing was completed, data were analyzed by breaking data into sections that represented the throw, return, and two stationary periods and were joined so that there were four single arrays to represent the yaw and pitch for the head and trunk.

4 Results

Figures 16, 17, and 18 display representative results for the response of the head and trunk during the throw periods.

Vel yaw: head (red) & trunk (blk)

Figure 16: Angular velocity (top) & power spectral density (bot)
for yaw motions of head (red) & trunk (blk) during throw

Vel pitch: head (blu) & trunk (grn)
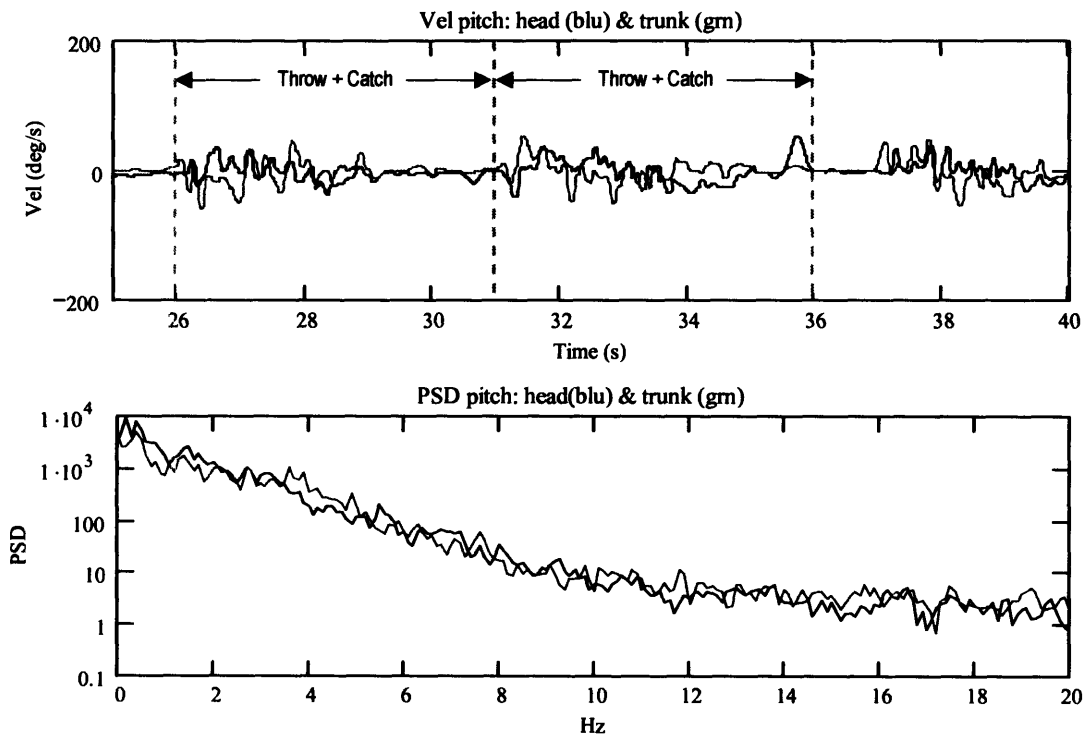
Figure 17: Angular velocity (top) & power spectral density (bot)
for pitch motions of head (blu) & trunk (grn)

These results are an example of the graphs created for all three sections of the data – throw, return, and stationary. From Figure 16, it is clear that in yaw the body moves at much higher magnitudes than the head. The trunk also has a higher spectral density throughout the range of frequencies higher than 1 Hz. In addition, there is a noticeable peak in the trunk yaw at around 2 Hz, which indicates how the subject's body moved with each step as they run toward the ball. In pitch, the magnitudes and spectral densities of both systems were much more similar than in the yaw direction (Figure 17). In both pitch and yaw, there is a three order of magnitude roll off displayed in the power spectral density from 0 to 10 Hz. Overall, the content is strongest at 0 to 2 Hz. Figure 18 displays that the magnitudes of velocity in the yaw and pitch direction are very similar for the head, but the yaw experiences much higher velocity in the trunk.
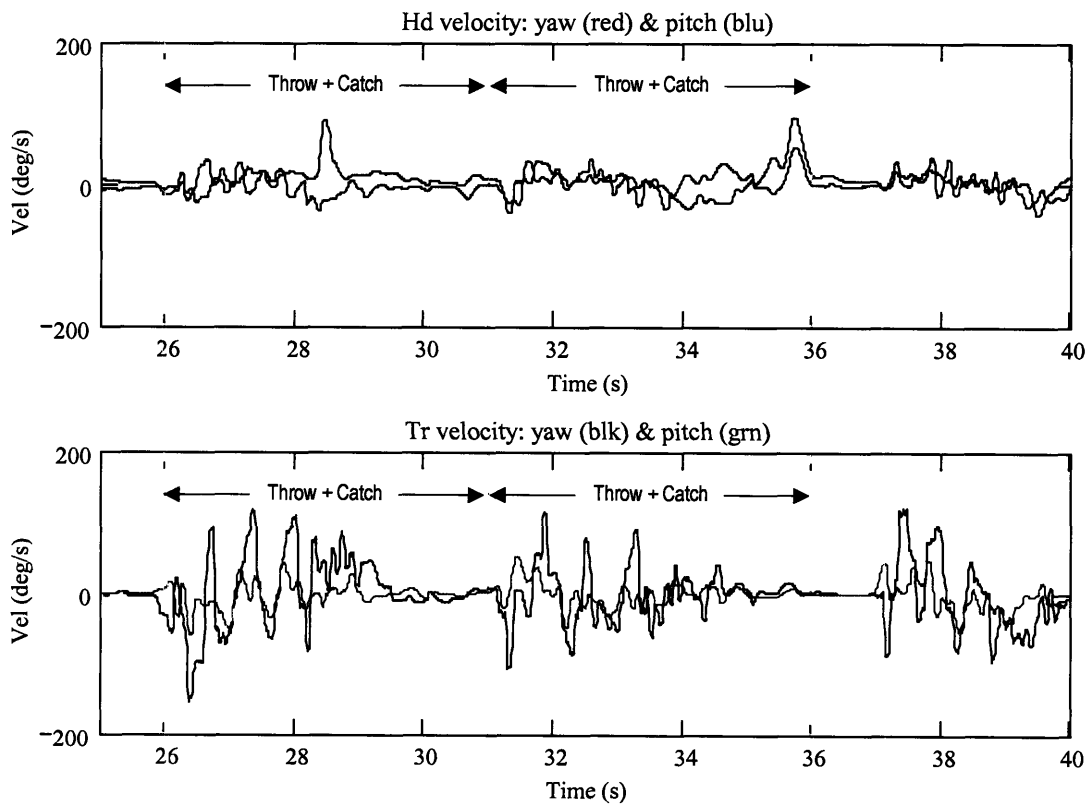
Figure 18: Head (top) & trunk (bot) velocities for yaw (red,blk and pitch (blu,grn) motions

During the return period, head and trunk velocities in the yaw direction were very similar. Figure 19 is a representative sample displaying one full return period and part of another. Notice that this return period is 8 seconds, which is 3 seconds longer than the throw periods mentioned above. This indicates that the subject's average speed during the return was slower than during the throw period since the same distance was covered. The spike at the start of the period is from the subject throwing the ball back to the experimenter and is repeated throughout the data set. There is still the three order of magnitude roll off in the power spectral density from 0 to 10 Hz.
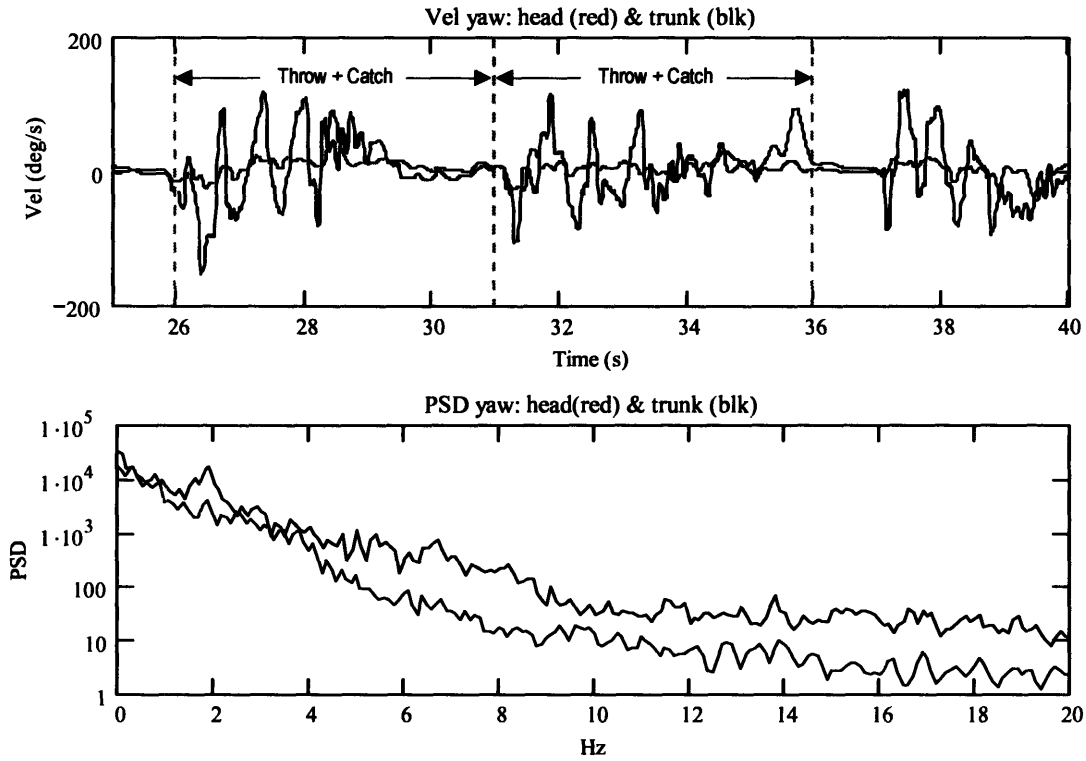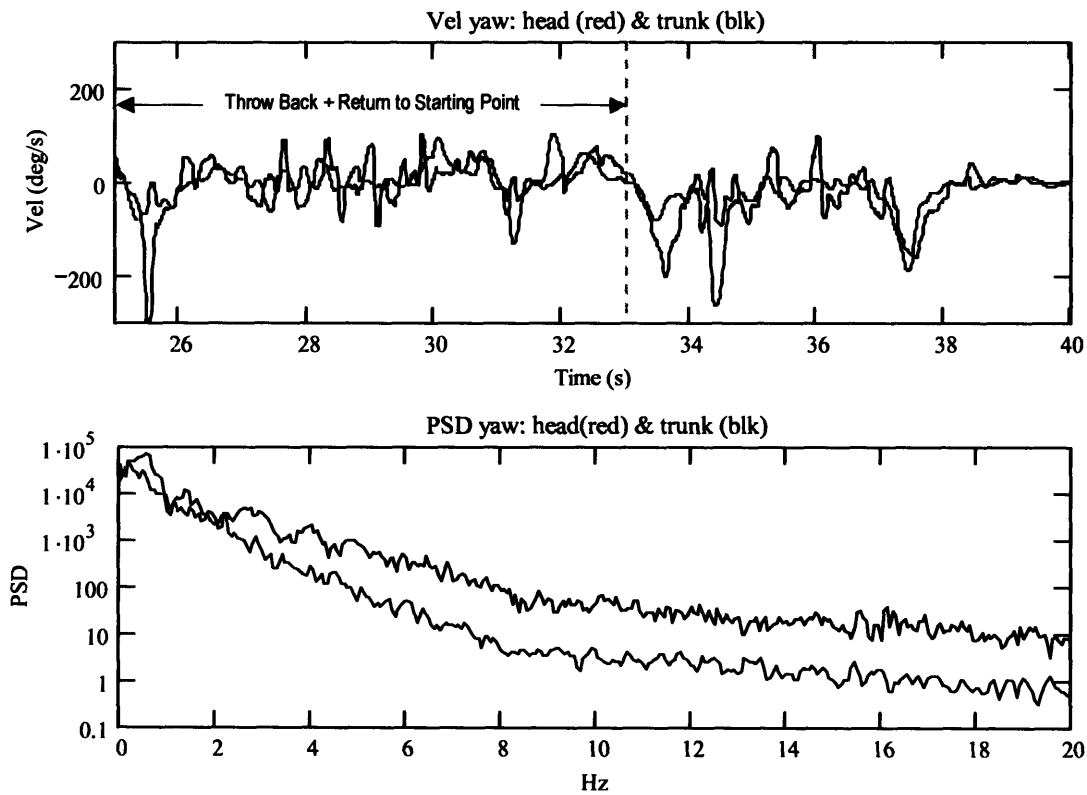

Figure 19: Figure 16: Angular velocity (top) & power spectral density (bot)
for yaw motions of head (red) & trunk (blk) during return

This analysis was repeated for the stationary period also. There were no surprises in this section. The magnitudes of velocities for head and trunk in all directions were extremely similar. The power spectral densities were almost equivalent also.

Overall, five trials were completed. Two sets of data were discarded because of experimental difficulties that prevented proper analysis in a manner similar to the others. Summary of the data for two of the analyzed data sets is shown in Table 2. It displays the root mean square (RMS) and maximum values of each value in each section. RMS was used as representative of the expected value of the magnitude. During all trials, head velocities rarely exceeded 160 deg/s in pitch and 200 deg/s in yaw, and trunk velocities rarely exceeded 90 deg/s in pitch and 200 deg/s in yaw.

Subject 1		RMS	Max
Throw	Hy	36.5	122
	Ty	50.2	164
	Hp	36.1	157
	Tp	21.1	90
Return	Hy	45.6	200
	Ty	57.4	205
	Hp	21.1	120
	Tp	23.2	60
Stationary	Hy	14.8	60
	Ty	11.2	55
	Hp	8.2	50
	Tp	4.4	28

Subject 2		RMS	Max
Throw	Hy	12.4	57
	Ty	28.1	113
	Hp	20.6	49
	Tp	15.5	56
Return	Hy	30.8	184
	Ty	35.1	156
	Hp	17.1	85
	Tp	11.9	45
Stationary	Hy	7	59
	Ty	7.1	52
	Hp	5.7	34
	Tp	4.4	35

Table 2: Summary of data from two subjects
Hy=Head Yaw; Ty=Trunk Yaw, Hp=Head Pitch, Tp=Trunk Pitch

5 Discussion

5.1 Design

The design of the experimental equipment successfully achieved our main design and experimental objectives of measuring angular velocity of the head and trunk during unrestrained, natural activities that require clear vision. The equipment allowed the subject to have a full range of motion while still maintaining a robust design. With strategic wire and connection placement, the subject trusted he or she would not damage

the equipment and was able to run as if not instrumented. Sometimes it took a trial for the subject to become comfortable with the equipment and trust that they could move without being constrained, but once convinced, the data appeared representative of natural motion. The trials continued, and data was still recorded accurately from the sensors thereby displaying the true sturdiness of design. Moreover, the ease of use of the DAQ software led to quick and efficient analysis. After recording data, the DAQ program written in LabVIEW allowed for easy data analysis. It placed the data from each of the four BNC connectors into a text file with four easily identifiable arrays. Using MathCAD, data could go from the tablet PC to readable graphs such as those in Figures 16-19 in a matter of minutes. This quick feedback was helpful in improving data collection from trial to trial.

Many improvements were made to the equipment based on feedback throughout the testing period, and more should be made to improve future data collection. A key design adjustment made during testing was mounting the junction box higher on the helmet. It had first been mounted at the bottom of the helmet resulting in the box and connectors colliding with the backpack when looking up. This resulted in the destruction of the junction box during the first set of testing. The solution of moving the box up along with the use of shrink wrap to strengthen the wiring lasted through the last trial.

It is recommended that future versions be made lighter in several ways so each subject can move at a running speed more similar to what it would be if not instrumented. Improvements include using a PDA or wireless sensors, constructing sensor boxes with thinner acrylic, shaving weight from the helmet, and using a smaller DAQ connection block. A PDA could collect the data during trials instead of a laptop as long as it houses

a PCMCIA or Compact Flash slot and the hard drive and memory capable of running LabVIEW. NI actually sells a version of LabVIEW that requires less computer power for exactly this application. So with the purchase of a PDA, NI's LabVIEW PDA module, and NI's Compact Flash data acquisition card, several pounds could be removed from the backpack. The data could be transferred from the PDA to a more powerful computer for analysis at some time after testing is completed. Being even more ambitious, wireless sensors could be developed to allow for remote data collection, and a backpack would not even be necessary. More feasible, near-term weight decreasing solutions could come from using thinner acrylic for the sensor boxes, cutting parts of the helmet that are unnecessary to maintain structural integrity, and using a smaller DAQ connection block. Specifically, the DAQ connection block chosen for this experiment (NI SCB-68) could be changed to a smaller, lighter model (NI CB-68LP) sold by National Instruments. The SCB-68 was initially selected because it has a prototyping board that allows filtering and bias resistors to be added for signal conditioning. After obtaining data, it was decided that the signal did not need additional conditioning. Therefore, a switch to NI CB-68LP would cause the size and weight of the backpack to decrease.

5.2 Protocol

The experimental protocol was designed to stimulate a large range of motions that included visual tasks, and it successfully achieved our main experimental objectives which were to simulate a natural event that requires clear vision. The protocol allowed for the subject to move and act as if not instrumented with the sensor and data acquisition systems. Moreover, it resulted in the ability to break down the data into the three main sections (throw, return, stationary).

Although there were some flaws at first, the execution of the experimental protocol improved with each trial as the experimenter and subject learned what worked best for data collection. The first trials were run with random timing so the subjects returned to the starting point whenever they wanted to. This created extra post-test work because it was tough to sift through the non-repetitive data and determine where each throw was made. The solution was simple – make throws and command the subject to return at certain time intervals. In this case, the experimenter made a throw every 20 seconds allowing each of these throws to be identified quickly from the data set. Ten seconds after each throw, the subjects were instructed to throw the ball back and return to the start position. Each throw and catch elapsed over a period of no more than 5 seconds; therefore there was about 5 seconds of stationary time after catching the ball. Furthermore, each return period lasted about 8 seconds; therefore there was a second stationary period of 2 seconds before the next throw took place. Each data section was identifiable thanks to the stationary times between every throw and return. The difference in length of the two types of stationary periods (5 seconds after the throw and 2 seconds after the return) allowed for further recognition of the data sections.

Looking forward, this research could easily be extended to different "natural" settings such as running on a track while chasing a target in front and running back-and-forth to hit a tennis ball. The current experimental equipment could be used for the running experiment without change. However, it would require some changes to handle a sport such as tennis. If the body were moving more violently from side to side, the weight of the backpack would be more critical since it may experience larger forces.

Also, the backpack and trunk sensor box would get in the way of a full tennis swing. The thought of this could cause the subject to inadvertently alter their normal dynamics.

5.3 Experimental Results

The research produced some interesting results that reinforced the main hypothesis in the yaw direction, but did the opposite in the pitch direction. We expected that moving while tracking an object would result in lower magnitude velocities in both yaw and pitch relative to motion without tracking. In yaw, head and trunk velocities were greatest when subjects ran without a defined visual task. Across subjects, the RMS of the head velocities averaged 38.2 deg/s, and for the trunk averaged 46.3 deg/s. The velocities of the head and trunk decreased considerably when subjects had to also track and catch the moving ball. The RMS head velocity decreased to 24.5 deg/s, and for the trunk decreased to 38.1 deg/s. This reduction was in spite of subjects running approximately 50% faster than when no visual task had been given, and likely reflects the need to stabilize the head against yaw motions to maintain clear vision. Surprisingly, the results were reversed for pitch velocities. Larger magnitude head and trunk velocities occurred in pitch when subjects ran and visually tracked the ball's trajectory than when subjects ran without the visual task (mean RMS of 23.4 deg/s and 18.3 deg/s vs. 19.1deg/s and 17.5deg/s). For all conditions, the frequency spectra of head and trunk velocities were dominated by power between 0.0 and 2.0 Hz, with the power spectral density dropping by more than three orders of magnitude by 10.0 Hz.

Some other observations were particularly interesting. If the subject was not trying to stabilize his or her head, the head moved very similar the body in the yaw direction (Figure 19). It is also not clear that head movement lags trunk movement,

which would be the intuitive assumption. The power spectral densities for the head and trunk in yaw and also in pitch are very similar up to 1 Hz. At about 2 Hz, there were peaks in the trunk power spectrum. This could help indicate the average speed of the subject during the experiment.

The ranges of velocities found in this experiment seem to agree with previous work on the subject. In particular, Grossman *et. al* (1988) found that 19 of 20 subjects never exceeded 170 deg/s in yaw or pitch while running. Pozzo *et. al* (1990) found these peak values to be less than 140 deg/s. The maximum numbers determined in our experiment were 160 deg/s in pitch and 200 deg/s in yaw. The higher yaw number can be attributed to the experimental design differences. Grossman and Pozzo each had the subjects run in place, while our experiment was designed to allow the subjects to move freely. This increased range of velocity recorded displays the importance of expanding vestibular system and human head dynamics research to a natural, unrestrained setting.

6 References

Fuller JH. Head movement propensity. Exp Brain Res. 92: 152-164, 1992.

Gong W, Merfeld DM. A prototype neural semicircular canal prosthesis using patterned electrical stimulation. Annals of Bio Eng. 28(5): 572-581, 2000.

Grossman GE, Leigh RJ, Abel LA, Lanska DJ, Thurston SE. Frequency and velocity of rotational head perturbations during locomotion. Exp Brain Res. 70(3): 470-6, 1988.

Hirasaki E, Moore ST, Raphan T, Cohen B. Effects of walking velocity on vertical head and body movements during locomotion. Exp Brain Res. 127(2): 117-130, July 1999.

Keshner EA, Hain TC, Chen KJ. Predicting control mechanisms for human head stabilization by altering the passive mechanics. J Vestib Res. 9: 423-434, 1999.

National Institutes of Health. A report of the task force on the national strategic research plan. National Institute on Deafness and Other Communication Disorders, Bethesda, Maryland. April 1989, 12, 74.

Peng GCY, Hain TC, Peterson BW. A dynamical model for reflex activated head movements in the horizontal plane. Biol Cybern. 75: 309-319, 1996.

Peterson, BW. Current approaches and future directions to understanding control of head movement. Progress in Brain Res. 143(35): 369-381, 2004.

Pozzo T, Berthoz A, Lefort L. Head stabilization during various locomotor tasks in humans. Exp Brain Res. 82: 97-106, 1990.

Pozzo T, Levik Y, Berthoz A. Head and trunk movements in the frontal plane during complex dynamic equilibrium tasks in humans. Exp Brain Res. 106(2): 327-338, 1995.

Pulaski PD, Zee DS, Robinson DA. The behavior of the vestibule-ocular reflex at high velocities of head rotation. Brain Res. 222: 159-165, 1981.

Whitton, Bob. Better military helmets studied. University of Waterloo news release, July 7, 1999. http://newsrelease.uwaterloo.ca/news.php?id=1255. May 11, 2006.

Wilson VJ, Boyle R, Fukushima K, Rose PK, Shinoda Y, Sugiuchi Y, Uchino Y. The vestibulocollic reflex. J Vestib Res. 5(3): 147-70, May-Jun 1995.

7 Appendix A

ANALOG DEVICES

±300°/s Single Chip Yaw Rate Gyro with Signal Conditioning

ADXRS300

FEATURES

Complete rate gyroscope on a single chip
Z-axis (yaw rate) response
High vibration rejection over wide frequency
2000 g powered shock survivability
Self-test on digital command
Temperature sensor output
Precision voltage reference output
Absolute rate output for precision applications
5 V single-supply operation
Ultrasmall and light (< 0.15 cc, < 0.5 gram)

APPLICATIONS

Vehicle chassis rollover sensing
Inertial measurement units
Platform stabilization

GENERAL DESCRIPTION

The ADXRS300 is a complete angular rate sensor (gyroscope) that uses Analog Devices' surface-micromachining process to make a functionally complete and low cost angular rate sensor integrated with all of the required electronics on one chip. The manufacturing technique for this device is the same high volume BIMOS process used for high reliability automotive airbag accelerometers.

The output signal, RATEOUT (1B, 2A), is a voltage proportional to angular rate about the axis normal to the top surface of the package (see Figure 4). A single external resistor can be used to lower the scale factor. An external capacitor is used to set the bandwidth. Other external capacitors are required for operation (see Figure 5).

A precision reference and a temperature output are also provided for compensation techniques. Two digital self-test inputs electromechanically excite the sensor to test proper operation of both sensors and the signal conditioning circuits. The ADXRS300 is available in a 7 mm × 7 mm × 3 mm BGA chip-scale package.
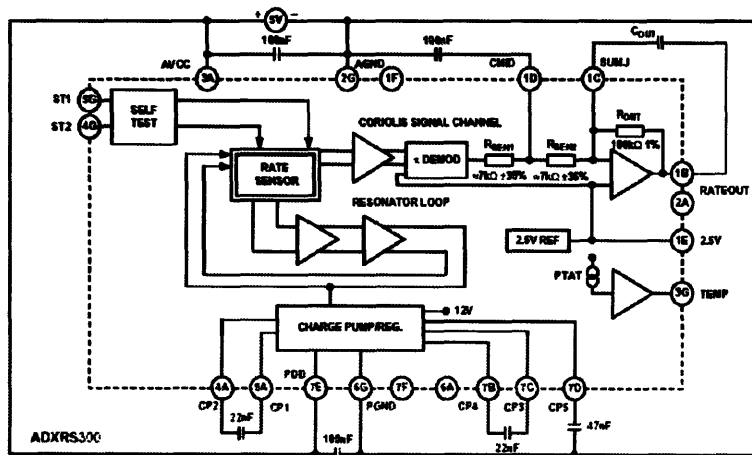
FUNCTIONAL BLOCK DIAGRAM

Figure 1.

ADXRS300

TABLE OF CONTENTS

REVISION HISTORY

SPECIFICATIONS

@T_A = 25°C, V_S = 5 V, Angular Rate = 0°/s, Bandwidth = 80 Hz (C_{OUT} = 0.01 µF), ±1g, unless otherwise noted.

Table 1.

Parameter	Conditions	ADXRS300ABG Min[1]	Typ	Max[1]	Unit
SENSITIVITY	Clockwise rotation is positive output				
Dynamic Range[2]	Full-scale range over specifications range	±300			°/s
Initial	@25°C	4.6	5	5.4	mV/°/s
Over Temperature[3]	V_S = 4.75 V to 5.25 V	4.6	5	5.4	mV/°/s
Nonlinearity	Best fit straight line		0.1		% of FS
NULL					
Initial Null		2.3	2.50	2.7	V
Over Temperature[3]	V_S = 4.75 V to 5.25 V	2.3		2.7	V
Turn-On Time	Power on to ±½°/s of final		35		ms
Linear Acceleration Effect	Any axis		0.2		°/s/g
Voltage Sensitivity	V_{CC} = 4.75 V to 5.25 V		1		°/s/V
NOISE PERFORMANCE					
Rate Noise Density	@25°C		0.1		°/s/√Hz
FREQUENCY RESPONSE					
3 dB Bandwidth (User Selectable)[4]	22 nF as comp cap (see the Setting Bandwidth section)		40		Hz
Sensor Resonant Frequency			14		kHz
SELF-TEST INPUTS					
ST1 RATEOUT Response[5]	ST1 pin from Logic 0 to 1	−150	−270	−450	mV
ST2 RATEOUT Response[5]	ST2 pin from Logic 0 to 1	+150	+270	+450	mV
Logic 1 Input Voltage	Standard high logic level definition	3.3			V
Logic 0 Input Voltage	Standard low logic level definition			1.7	V
Input Impedance	To common		50		kΩ
TEMPERATURE SENSOR					
V_{OUT} at 298°K			2.50		V
Max Current Load on Pin	Source to common			50	µA
Scale Factor	Proportional to absolute temperature		8.4		mV/°K
OUTPUT DRIVE CAPABILITY					
Output Voltage Swing	I_{OUT} = ±100 µA	0.25		V_S − 0.25	V
Capacitive Load Drive		1000			pF
2.5 V REFERENCE					
Voltage Value		2.45	2.5	2.55	V
Load Drive to Ground	Source		200		µA
Load Regulation	0 < I_{OUT} < 200 µA		5.0		mV/mA
Power Supply Rejection	4.75 V_S to 5.25 V_S		1.0		mV/V
Temperature Drift	Delta from 25°C		5.0		mV
POWER SUPPLY					
Operating Voltage Range		4.75	5.00	5.25	V
Quiescent Supply Current			6.0	8.0	mA
TEMPERATURE RANGE					
Specified Performance Grade A	Temperature tested to max and min specifications	−40		+85	°C

[1] All minimum and maximum specifications are guaranteed. Typical specifications are not tested or guaranteed.
[2] Dynamic range is the maximum full-scale measurement range possible, including output swing range, initial offset, sensitivity, offset drift, and sensitivity drift at 5 V supplies.
[3] Specification refers to the maximum extent of this parameter as a worst-case value of T_{MIN} or T_{MAX}.
[4] Frequency at which response is 3 dB down from dc response with specified compensation capacitor value. Internal pole forming resistor is 180 kΩ. See the Setting Bandwidth section.
[5] Self-test response varies with temperature. See the Self-Test Function section for details.

ABSOLUTE MAXIMUM RATINGS

Table 2.

Parameter	Rating
Acceleration (Any Axis, Unpowered, 0.5 ms)	2000 g
Acceleration (Any Axis, Powered, 0.5 ms)	2000 g
+Vs	–0.3 V to +6.0 V
Output Short-Circuit Duration (Any Pin to Common)	Indefininte
Operating Temperature Range	–55°C to +125°C
Storage Temperature	–65°C to +150°C

Stresses above those listed under the Absolute Maximum Ratings may cause permanent damage to the device. This is a stress rating only; functional operation of the device at these or any other conditions above those indicated in the operational section of this specification is not implied. Exposure to absolute maximum rating conditions for extended periods may affect device reliability.

Applications requiring more than 200 cycles to MIL-STD-883 Method 1010 Condition B (-55°C to +125°C) require underfill or other means to achieve this requirement.

Drops onto hard surfaces can cause shocks of greater than 2000 g and exceed the absolute maximum rating of the device. Care should be exercised in handling to avoid damage.

RATE SENSITIVE AXIS

This is a Z-axis rate-sensing device that is also called a yaw rate sensing device. It produces a positive going output voltage for clockwise rotation about the axis normal to the package top, i.e., clockwise when looking down at the package lid.
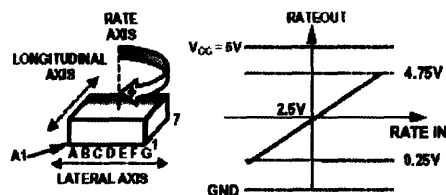
Figure 2. RATEOUT Signal Increases with Clockwise Rotation

ESD CAUTION

ESD (electrostatic discharge) sensitive device. Electrostatic charges as high as 4000 V readily accumulate on the human body and test equipment and can discharge without detection. Although this product features proprietary ESD protection circuitry, permanent damage may occur on devices subjected to high energy electrostatic discharges. Therefore, proper ESD precautions are recommended to avoid performance degradation or loss of functionality.

PIN CONFIGURATION AND FUNCTION DESCRIPTIONS
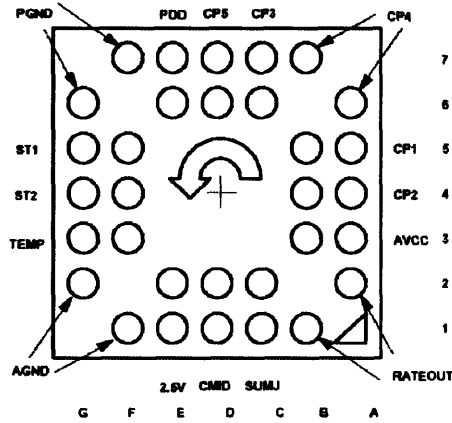
Figure 3. 32-Lead BGA (Bottom View)

Table 3. Pin Function Descriptions

Pin No.	Mnemonic	Description
6D, 7D	CP5	HV Filter Capacitor—47 nF
6A, 7B	CP4	Charge Pump Capacitor—22 nF
6C, 7C	CP3	Charge Pump Capacitor—22 nF
5A, 5B	CP1	Charge Pump Capacitor—22 nF
4A, 4B	CP2	Charge Pump Capacitor—22 nF
3A, 3B	AVCC	+ Analog Supply
1B, 2A	RATEOUT	Rate Signal Output
1C, 2C	SUMJ	Output Amp Summing Junction
1D, 2D	CMID	HF Filter Capacitor—100 nF
1E, 2E	2.5V	2.5 V Precision Reference
1F, 2G	AGND	Analog Supply Return
3F, 3G	TEMP	Temperature Voltage Output
4F, 4G	ST2	Self-Test for Sensor 2
5F, 5G	ST1	Self-Test for Sensor 1
6G, 7F	PGND	Charge Pump Supply Return
6E, 7E	PDD	+ Charge Pump Supply

ADXRS300

THEORY OF OPERATION

The ADXRS300 operates on the principle of a resonator gyro. Two polysilicon sensing structures each contain a dither frame, which is electrostatically driven to resonance. This produces the necessary velocity element to produce a Coriolis force during angular rate. At two of the outer extremes of each frame, orthogonal to the dither motion, are movable fingers that are placed between fixed pickoff fingers to form a capacitive pickoff structure that senses Coriolis motion. The resulting signal is fed to a series of gain and demodulation stages that produce the electrical rate signal output. The dual-sensor design rejects external g-forces and vibration. Fabricating the sensor with the signal conditioning electronics preserves signal integrity in noisy environments.

The electrostatic resonator requires 14 V to 16 V for operation. Since only 5 V is typically available in most applications, a charge pump is included on-chip. If an external 14 V to 16 V supply is available, the two capacitors on CP1-CP4 can be omitted and this supply can be connected to CP5 (Pin 7D) with a 100 nF decoupling capacitor in place of the 47 nF.

After the demodulation stage, there is a single-pole low-pass filter consisting of an internal 7 kΩ resistor (R_{SEN1}) and an external user-supplied capacitor (CMID). A CMID capacitor of 100 nF sets a 400 Hz ±5% low-pass pole and is used to limit high frequency artifacts before final amplification. The band-width limit capacitor, C_{OUT}, sets the pass bandwidth (see Figure 5 and the Setting Bandwidth section).

NOTE THAT INNER ROWS/COLUMNS OF PINS HAVE BEEN OMITTED FOR CLARITY BUT SHOULD BE CONNECTED IN THE APPLICATION.

Figure 4. Example Application Circuit (Top View)

SUPPLY AND COMMON CONSIDERATIONS

Only power supplies used for supplying analog circuits are recommended for powering the ADXRS300. High frequency noise and transients associated with digital circuit supplies may have adverse effects on device operation.

Figure 4 shows the recommended connections for the ADXRS300 where both AVCC and PDD have a separate decoupling capacitor. These should be placed as close to the their respective pins as possible before routing to the system analog supply. This minimizes the noise injected by the charge pump that uses the PDD supply.

It is also recommended to place the charge pump capacitors connected to the CP1-CP4 pins as close to the part as possible. These capacitors are used to produce the on-chip high voltage supply switched at the dither frequency at approximately 14 kHz. Care should be taken to ensure that there is no more than 50 pF of stray capacitance between CP1-CP4 and ground. Surface-mount chip capacitors are suitable as long as they are rated for over 15 V.

Figure 5. Block Diagram with External Components

SETTING BANDWIDTH

External capacitors CMID and C_{OUT} are used in combination with on-chip resistors to create two low-pass filters to limit the bandwidth of the ADXRS300's rate response. The -3 dB frequency set by R_{OUT} and C_{OUT} is

$$f_{OUT} = 1/(2 \times \pi \times R_{OUT} \times C_{OUT})$$

and can be well controlled since R_{OUT} has been trimmed during manufacturing to be 180 kΩ ± 1%. Any external resistor applied between the RATEOUT (1B, 2A) and SUMJ (1C, 2C) pins results in

$$R_{OUT} = (180 \text{ k}\Omega \times R_{EXT})/(180 \text{ k}\Omega + R_{EXT})$$

The -3 dB frequency is set by RSEN (the parallel combination of R_{SEN} and R_{SEN2}) at about 3.5 kΩ nominal; CMID is less well controlled since R_{SEN} and R_{SEN2} have been used to trim the rate sensitivity during manufacturing and have a ±35% tolerance. Its primary purpose is to limit the high frequency demodulation artifacts from saturating the final amplifier stage. Thus, this pole of nominally 400 Hz @ 0.1 μF need not be precise. Lower frequency is preferable, but its variability usually requires it to be about 10 times greater (in order to preserve phase integrity) than the well-controlled output pole. In general, both -3 dB filter frequencies should be set as low as possible to reduce the amplitude of these high frequency artifacts and to reduce the overall system noise.

INCREASING MEASUREMENT RANGE

The full-scale measurement range of the ADXRS300 can be increased by placing an external resistor between the RATEOUT (1B, 2A) and SUMJ (1C, 2C) pins, which would parallel the internal R_{OUT} resistor that is factory-trimmed to 180 kΩ. For example, a 330 kΩ external resistor will give ~50% increase in the full-scale range. This is effective for up to a 4× increase in the full-scale range (minimum value of the parallel resistor allowed is 45 kΩ). Beyond this amount of external sensitivity reduction, the internal circuitry headroom requirements prevent further increase in the linear full-scale output range. The drawbacks of modifying the full-scale range are the additional output null drift (as much as 2°/sec over temperature) and the readjustment of the initial null bias (see the Null Adjust section).

USING THE ADXRS300 WITH A SUPPLY-RATIOMETRIC ADC

The ADXRS300's RATEOUT signal is nonratiometric, i.e., neither the null voltage nor the rate sensitivity is proportional to the supply. Rather they are nominally constant for dc supply changes within the 4.75 V to 5.25 V operating range. If the ADXRS300 is used with a supply-ratiometric ADC, the ADXRS300's 2.5 V output can be converted and used to make corrections in software for the supply variations.

NULL ADJUST

Null adjustment is possible by injecting a suitable current to SUMJ (1C, 2C). Adding a suitable resistor to either ground or to the positive supply is a simple way of achieving this. The nominal 2.5 V null is for a symmetrical swing range at RATEOUT (1B, 2A). However, a nonsymmetric output swing may be suitable in some applications. Note that if a resistor is connected to the positive supply, then supply disturbances may reflect some null instabilities. Digital supply noise should be avoided, particularly in this case (see the Supply and Common Considerations section).

The resistor value to use is approximately

$$R_{NULL} = (2.5 \times 180,000)/(V_{NULLO} - V_{NULL1})$$

V_{NULLO} is the unadjusted zero rate output, and V_{NULL1} is the target null value. If the initial value is below the desired value, the resistor should terminate on common or ground. If it is above the desired value, the resistor should terminate on the 5 V supply. Values are typically in the 1 MΩ to 5 MΩ range.

If an external resistor is used across RATEOUT and SUMJ, then the parallel equivalent value is substituted into the preceding equation. Note that the resistor value is an estimate since it assumes $V_{CC} = 5.0$ V and $V_{SUM} = 2.5$ V.

SELF-TEST FUNCTION

The ADXRS300 includes a self-test feature that actuates each of the sensing structures and associated electronics in the same manner as if subjected to angular rate. It is activated by standard logic high levels applied to inputs ST1 (5F, 5G), ST2 (4F, 4G), or both. ST1 causes a voltage at RATEOUT equivalent to typically -270 mV, and ST2 causes an opposite +270 mV change. The self-test response follows the viscosity temperature dependence of the package atmosphere, approximately 0.25%/°C.

Activating both ST1 and ST2 simultaneously is not damaging. Since ST1 and ST2 are not necessarily closely matched, actuating both simultaneously may result in an apparent null bias shift.

CONTINUOUS SELF-TEST

The one-chip integration of the ADXRS300 gives it higher reliability than is obtainable with any other high volume manufacturing method. Also, it is manufactured under a mature BIMOS process that has field-proven reliability. As an additional failure detection measure, power-on self-test can be performed. However, some applications may warrant continuous self-test while sensing rate. Application notes outlining continuous self-test techniques are also available on the Analog Devices website.

OUTLINE DIMENSIONS

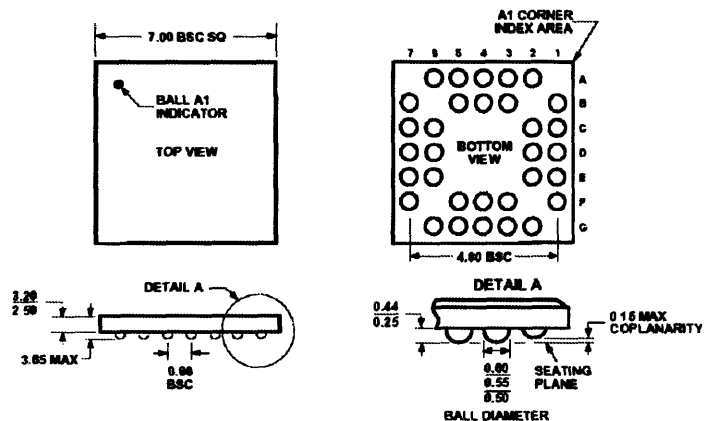Figure 6. 32-Lead Chip Scale Ball Grid Array (CSPBGA)
(BC-32)
Dimensions shown in millimeters

ORDERING GUIDE

Model	Temperature Range	Package Description	Package Outline
ADXRS300ABG	−40°C to +85°C	32-Lead BGA	BC-32
ADXRS300ABG-Reel	−40°C to +85°C	32-Lead BGA	BC-32
ADXRS300EB		Evaluation Board	

ANALOG
DEVICES

www.analog.com

8 Appendix B

ANALOG DEVICES

±300°/s Single Chip Rate Gyro Evaluation Board

ADXRS300EB

GENERAL DESCRIPTION

The ADXRS300EB is a simple evaluation board that allows the user to quickly evaluate the performance of the ADXRS300ABG rate gyros. No additional external components are required for operation. The ADXRS300EB has a 20-lead dual-in-line (0.3 inch width) by 0.1 inch pin spacing interface that allows the user to easily prototype products without having to deal with BGA soldering. The 0.1 square inch outline of the ADXRS300EB is still among the smallest gyros available today.

CIRCUIT DESCRIPTION

The schematic of the ADXRS300EB is shown in Figure 1. It is identical to the suggested application shown in the ADXRS300ABG data sheet.

The analog and power grounds (AGND and PGND) have separate ground planes and are joined at one point. The user may cut this trace if separate ground schemes are desired.

Note that the analog supply voltage and charge pump supply voltage (AVCC and PDD) are not connected on the ADXRS300EB, and the user must connect these as appropriate to the application.

The parts layout of the ADXRS300EB is shown in Figure 2, and the part list for the ADXRS300EB is shown in Table 1. As delivered, the ADXRS300EB is set for 40 Hz bandwidth (C = 22 nF). The user may add an additional external capacitor to further reduce the bandwidth and improve the noise floor.

SPECIAL NOTES ON HANDLING

Note that the ADXRS300EB is not reverse polarity protected. Reversing the power supply, or applying inappropriate voltages to any pin outside the ADXRS300 data sheet's Absolute Maximum Ratings, may damage the ADXRS300EB.
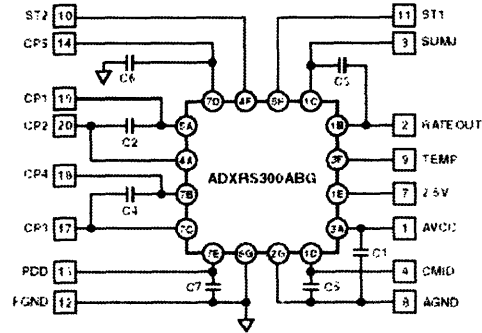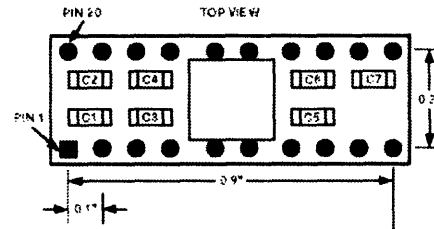

Figure 1. ADXRS300EB Schematic

Figure 2. ADXRS300EB Parts Layout

Table 1. ADXRS300EB Component Values

Component	Values (nF)
C1	100
C2	22
C3	22
C4	22
C5	100
C6	17
C7	100

C03540-0-1 03/0)

PRINTED IN U.S.A

41

9 Appendix C

$1.59

+5V Fixed-Voltage Regulator 7805
Model: 7805 | Catalog #: 276-1770

This high-power regulator has capabilities up to +5V at 1 amp.

Customers rate it: ★ ★ ★ ★ ★   Wish List   🛒 Add to cart   › Order online with peace of mind

Online: ■ In stock · Usually **ships** in 1-2 business days | In store: Available at most stores, find it near you

Free shipping on orders of $50 or more ›More details

Tech specs

Dimensions

Product Length	0

General Features

Model	7805
Product Type	IC-Analog
Enclosure Color	Black

Fits What

Model	7805

Miscellaneous Features

Supported Languages	English
Mounting Kit	Case style: TO-220
#per pack	1

Power Features

Power Device	Output Voltage: +5VDC @ 1A Maximum Input Voltage: 35VDC
Voltage Required	Maximum Input Voltage: 35VDC

Battery Features

10 Appendix D

5.6 Energy Density

Energy density is a measure of available energy in terms of weight and volume. It is the ratio of a cell's capacity to either its volume or weight and can be used to evaluate a cell's performance.

Table 1 is a summary of the major alkaline product types comparing both volumetric energy density and gravimetric energy density. Volumetric energy density

is an important factor where battery size is the primary design consideration. Gravimetric energy density becomes important where weight of the battery is critical, such as in portable computers and cellular phones. The values shown in this table are typical for each cell size. Actual energy output will vary, dependent mostly on drain rates applied.

PRODUCT NUMBER	SIZE	NOMINAL VOLTAGE volts	RATED CAPACITY* ampere-hours	LOAD ohms	WEIGHT		VOLUME		TYPICAL GRAVIMETRIC ENERGY DENSITY**		TYPICAL VOLUMETRIC ENERGY DENSITY	
					pounds	kilograms	cubic inches	liters	watt-hours per pound	watt-hours per kilogram	watt-hours per cubic inch	watt-hours per liter
MN1500	D	1.5	15.000	10	0.304	0.138	3.440	0.056	59.2	130	5.2	422
MN1400	C	1.5	7.500	20	0.143	0.065	1.640	0.027	63.3	111	5.7	317
MN1500	AA	1.5	2.850	43	0.052	0.024	0.510	0.008	65.8	143	6.7	428
MN2400	AAA	1.5	1.150	75	0.024	0.011	0.230	0.004	57.5	126	6.0	345
MN9100	N	1.5	0.800	100	0.021	0.010	0.210	0.003	45.7	96	4.5	320
7K67	J	6.0	0.580	340	0.075	0.034	0.960	0.016	37.2	82	2.9	174
MN908	Lantern	6.0	11.500	15	1.349	0.612	30.620	0.502	40.9	90	1.8	110
MN918	Lantern	6.0	24.000	9	2.800	1.270	75.880	1.243	41.1	91	1.5	93
MN1604	9V	9.0	0.580	620	0.101	0.046	1.390	0.023	41.4	91	3.0	182

* To 0.8V per cell at 21°C (70°F).
** Based on 1.2 volt average operating voltage per cell at 21°C (70°F).

Table 1. Comparison of typical energy densities of major DURACELL alkaline cells/batteries.

To determine the practical energy density of a cell under specific conditions of load and temperature, multiply the ampere-hour capacity that the cell delivers under those conditions by the average discharge voltage, and divide by cell volume or weight.

Gravimetric Energy Density:

$$\frac{\text{(Drain in Amperes x Service Hours)} \times \text{Average Discharge Voltage}}{\text{Weight of cell in Pounds or Kilograms}} = \frac{\text{Watt-Hours}}{\text{Pound or Kilogram}}$$

Volumetric Energy Density:

$$\frac{\text{(Drain in Amperes x Service Hours)} \times \text{Average Discharge Voltage}}{\text{Volume of cell in Cubic Inches or Liters}} = \frac{\text{Watt-Hours}}{\text{cubic Inch or Liter}}$$

Using the MN1300 data from **Table 1** the previous equations can be used to determine energy density for this cell

Gravimetric Energy Density:

$$\frac{15.00 \text{ Ampere-Hours} \times 1.2 \text{ Volts}}{0.304 \text{ Pounds (0.138 Kilograms)}} = \frac{59.2}{\text{Watt-Hours}} \text{ or } \frac{130.4}{\text{Watt-Hours}}$$
$$\text{Pound} \qquad \text{Kilogram}$$

Volumetric Energy Density:

$$\frac{15.00 \text{ Ampere-Hours} \times 1.2 \text{ Volts}}{3.44 \text{ Cubic Inches (0.563 Liters)}} = \frac{5.23}{\text{Watt-Hours}} \text{ or } \frac{320}{\text{Watt-Hours}}$$
$$\text{Cubic Inch} \qquad \text{Liter}$$